Journal of Ovonic Research Vol. 17, No. 2, March - April 2021, p. 165 - 173

ENHANCED STRUCTURAL AND ELECTRICAL PROPERTIES OF Ca-Ba RARE EARTH SUBSTITUTED M –TYPE HEXAFERRITES

H. M. KHAN[a], S. MUMTAZ[b], A. WAHEED[c], J. AHMAD[d], M. E. MAZHAR[d,*], W. ABBAS[d], I. KHAN[d], M. N. USMANI[d], S. BAKHTAWARA[d], A. JAVED[d], G. A. ASHRAF[e], S. AHMAD[d], R. NAZ[e], S. AHMAD[f]

[a]*Department of Physics, Islamia University Bahawalpur, Bahawalpur-63100, Pakistan*

[b]*Department of Physics, Allama Iqbal Open University, Islamabad, Pakistan*

[c]*Department of Geotechnical Engineering, MCE (NUST), Risalpur, Pakistan*

[d]*Department of Physics, Bahauddin Zakariya University, Multan, Pakistan*

[e]*School of Material Science and Engineering, Shanghai Jao Tong University, Dongchuan Road, Shanghai, 200240, P. R. China*

[f]*Department of Civil Engineering, UCE&T, Bahauddin Zakariya University, Multan, Pakistan*

Effect of Indium-Manganese (In-Mn) substitution on the structural electrical and dielectric properties of $Ca_{0.5-x}$ $Ba_{0.5}In_xMn_yFe_{12-y}O_{19}$ (x = 0.00–0.10; y= 0.00–1.00) hexaferrites prepared by sol–gel auto combustion method was reported. As-synthesized samples were characterized by Fourier transform infrared spectroscopy (FTIR), X-ray diffraction (XRD), scanning electron microscopy (SEM), and electrical and dielectric properties (resistivity and conductivity). The X-ray diffraction analysis confirmed the formation of M-type hexa-ferrite structure. A slight enhancement was found in the in-plane lattice constant *a*, while the lattice constant *c* was suppressed with the increasing concentration of In and Mn. The results of SEM images show that the grain size decreases with increase of In-Mn substitution from 10μm to 1μm. The increased dielectric properties and fine particle sizes are useful for many applications, such as cores of inductors, transformers, isolators and magnetic memory devices.

(Received December 4, 2020; Accepted March 17, 2021)

Keywords: FTIR, XRD, SEM, Electrical properties, M Type Hexaferrite, Sol - gel, Dielectric properties

1. Introduction

Ferrites are revolutionizing the functionality of the systems of materials. Ferrites are thought to be attractive type of magnetic materials having applications in special devices such as cores of a transformer, isolators, noise filter and magnetic memories, magnetic recording media, permanent magnets, and magneto-optical devices. A lot of studies on the magnetic properties of hexagonal ferrites have been reported, which shows enhanced magnetic, structural and microwave properties due to the combination of rare earth elements [1–4].

The hexaferrite materials have enhanced production of such devices and their effectiveness at the commercial level. The importance of hexaferrites is due to easy manufacturing, low cost, high power and low loss. The nano-sized $CaBaFe_{12}O_{19}$ M-type hexaferrite, have a single magnetic domain and high anisotropy, owing this they exhibit excellent magnetic properties [5–9]. As communication and electronic systems are moving toward higher working frequencies, hexaferrites materials are highly demanded as compared to the spinel ferrites. Therefore, hexaferrites are promising candidate for devices that operate in microwave frequencies, for example, microwave absorbers. The intrinsic magnetic properties resulted from the specific site occupancy of the Fe ions and rear earth (RE) elements at the side of divalent cations that enhance

* Corresponding author: dr.ehsan@bzu.edu.pk

the magnetic properties of ferrites [10, 11]. These reasons make the manipulation of Fe and RE in the lattices, as a promising way to improve electric and dielectric properties of hexagonal ferrites. The electrical properties like activation energy (ΔE) and ac conductivity (σ_{ac}) reveal very novel information concerning the effectiveness of these materials for many applications [12].

In our recent work, the sol-gel method has been used to synthesis In-Mn substituted calcium barium hexaferrites, to the best of our knowledge, no work has been reported until now on such nanocomposite. High electrical resistivity and low dielectric losses are obtained from as-synthesized nanomaterial in this study and that are useful for many applications such as recording media, optical waveguides, microwave absorption, and permanent magnets.

2. Experimental procedure

2.1. Sample preparation

In this study, M-type nano-hexaferrites $Ca_{0.5-x}Ba_{0.5}In_xMn_yFe_{12-y}O_{19}$, (x = 0.00 – 0.10 and y = 0.00–1.00) were prepared by sol–gel auto combustion method [17]. All analytic grade chemicals were purchased from Sigma-Aldrich company. Firstly, weighted amount of citric acid and iron chloride $Fe(NO_3)_2.9H_2O$, calcium chloride $CaCl_2$, barium nitrate $Ba(NO_3)_2$, manganese chloride $MnCl_2.4H_2O$, $C_6H_8O_7$, indium nitrate $In(NO_3)_3.H_2O$ each were dissolved in 100 ml of deionized water separately. Next, stoichiometric amount of solutions were mixed to prepared series of $Ca_{0.5-x}Ba_{0.5}In_xMn_yFe_{12-y}O_{19}$, (x = 0.00 – 0.10 and y = 0.00–1.00) samples. The solution was then magnetically stirred for 6 to 8 hours on magnetic hot plate at 80°C. To maintain the PH value, ammonia solution was added drop wise in reaction mixture several time. After 6 to 8 h reaction, solution was converted into gel and gel was burnt to ashes through auto-combustion at high temperature. Then, obtained ashes were dried at 300 °C by placing in oven for 2 hours. The nanomaterial was then grounded in agate mortar and pestle for 30 minutes to get fine powder. The powder was homogenized in furnace at temperature 900 °C for 9 hours. The pellets of as-synthesized nanomaterial with 8mm in diameter and 20 mm thickness were also formed at 80 KN by using Paul-Otto Weber Hydraulic Press. Finally, the pellets were sintered at 900 °C for 5 h.

3. Results and discussion

3.1. X-ray diffraction analysis

Fig. 1 shows the X- ray diffraction (XRD) patterns of $Ca_{0.5-x}Ba_{0.5}In_xMn_yFe_{12-y}O_{19}$, (x = 0.00 - 0.10 and y = 0.0 - 1.00) Hexaferrites. The peaks were identified and compared with standard data (JCPDS card No. 01-078-0132). The patterns match very well with standard pattern of barium hexaferrite, having different planes (103), (003), (102), (111), (114), (107), (202), (004), (111), (220) and (311) at 2θ of 20.6°, 24.2° , 27.7°, 32.38°, 33.31°, 34.2°, 35.7°, 41.0°, 49.7°, 54.0° and 64.20° respectively for lower concentration of In-Mn upto x = 0.6, however for higher concentrations we observed some additional peaks for 2 Θ value between 10 to 20°.

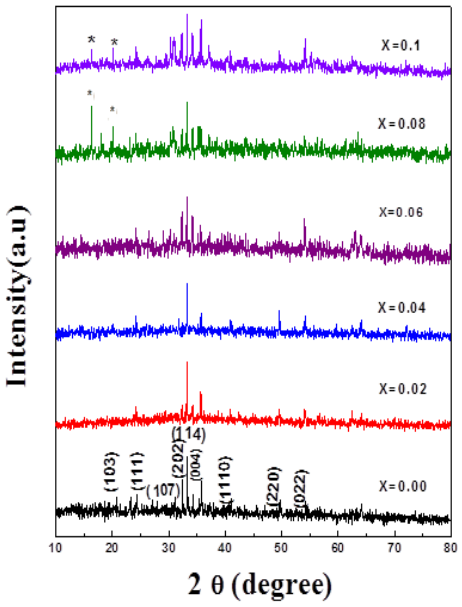

Fig. 1. XRD Pattern of $Ca_{0.50-x}Ba_{0.5}In_xMn_yFe_{12-y}O_{19}$ (x = 0.00 – 0.10 and y = 0.0 – 1.0) annealed at 900°C.

These peaks were referred to as the secondary phases. This may be attributed to the lower sintering temperature. All pattern showed hexagonal arrangement by arbitrary directions. By using the Debby Sharer's formula, the grain size [80] of samples were calculated from the line expansion of standard peaks of (114), (111) and (107) pattern. The value of lattice constants for ($Ca_{0.5-x}Ba_{0.5}In_xMn_yFe_{12-y}O_{19}$ (x = 0.00 – 0.10 and y = 0.00 –1.00) using equation (1) ,(2) are calculated *a* = 5.85Å and c = 23.32Å [27]. These values match very well with literature [28].

$$1/d^2 = 4/3(h^2 + k^2 + l^2)/a^2 + l^2/c^2 \quad (1)$$

$$d = \frac{a}{\sqrt{h2+k2+l2}} \quad (2)$$

where h, k and l are miller indices, d is interplanar spacing. The slight change in lattice constants is attributed to the difference among ionic radii of Fe^{3+} (0.645 Å), In^{3+}(0.80Å). The increase in lattice constants by substitution of different RE have been already reported [29,30]. Therefore, variation of lattice parameter and grain size indicated that In^{3+} has entered directly in the lattice of the hexa-ferrite [31]. The variation in the lattice constants *a* and *c* with In-Mn concentration is shown in Fig. 2. All the respective parameters of crystal structure have been reported in Tables 1 and 2.

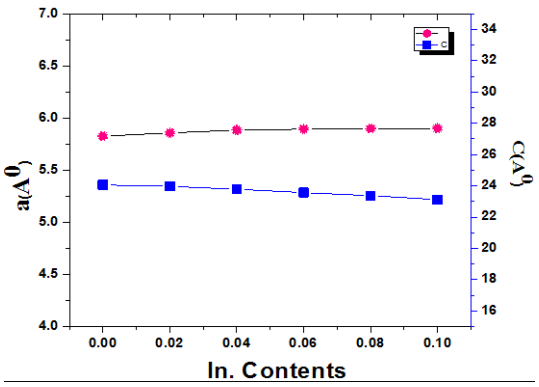

Fig. 2. Lattice parameters for $Ca_{0.5-x}Ba_{0.5}In_xMn_yFe_{12-y}O_{19}$ (x=0.00 – 0.10 and y= 0.00 -1.00) annealed at 900°C.

3.2. FTIR

Fig. 3 Shows the FTIR spectrum of M- type ($CaBaFe_{12}O_{19}$) in the range of 400-4000 cm^{-1}.The bands at 3539 cm^{-1} are due to near O-H stretch vibrations of physical absorbed water. The peak at 2036-2164 cm^{-1} is due to O=C=O of distinctive CO_2, whereas the peak at 1554 cm^{-1}assigned to O-H bending vibrations of physically adsorbed water. Many peaks assigned to M-O bonds were observed in the range of 1102- 500 cm^{-1}. The peak at 728 cm^{-1} is due to M-O bond of calcined M- Type ($Ca,Ba,Fe_{12}O_{19}$)[24-26].

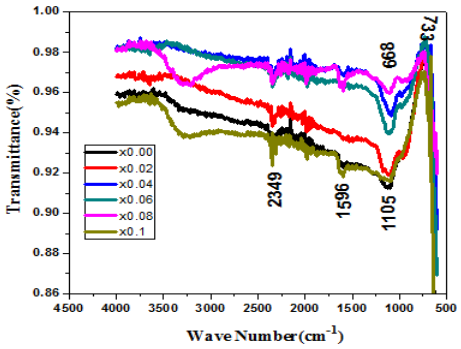

Fig. 3. FTIR spectrums for $Ca_{0.50-x}Ba_{0.5}In_x\ Mn_y\ Fe_{12-y}\ O_{19}$ (x = 0.00 – 0.10 and y = 0.0 – 1.0) annealed at 900°C.

4. Electrical properties

4.1. Room temperature resistivity

Fig. 4 shows the plot of room temperature electrical resistivity with increasing concentration of In-Mn. From the Fig. it is clear that the electrical resistivity increases with In^{3+} and Mn^{2+} ion concentrations. It is well known that the conductivity in hexaferrites is mainly due to the transfer of electron between Fe^{2+} and Fe^{3+} at the octahedral sites. Due to In-Mn doping the electrical resistivity increases in the range of $2.0x10^6$ (Ω-cm) to $5.7x10^6$(Ω-cm). The increase in electrical resistivity could be due to the formation of localized stable pair (Mn^{3+}, Fe^{2+}). The formation of Mn^{3+} will hinder the electron hopping between Fe^{2+} and Fe^{3+} to a greater extent. Furthermore, the room temperature electrical resistivity of Mn (160 $\times10^{-6}$ Ω cm) is larger than Fe (9.1 $\times$ 10^{-6} Ω cm). Due to these reasons an enhancement was found in the electrical resistivity of In-Mn doped systems as shown in Fig. 4.

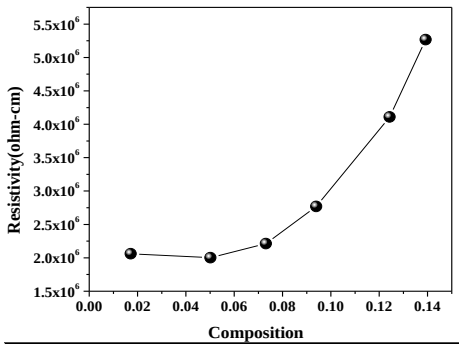

Fig. 4.Electrical resistivity at room temperature for $Ca_{0.5-x}Ba_{0.5}\ In_xMn_yFe_{12-y}O_{19}$ (x=0.00 – 0.10 and y= 0.0 -1.0).

4.2. Activation energy

The variation of electrical resistivity with temperature is calculated by following equation.

$$\rho=\rho_O \exp\frac{\Delta E}{K_B T} \quad (11)$$

The Fig. 5 show the plot of activation energy (ΔE) calculated from Arrhenius type equation. It is experimentally proved that the sample with high resistivity will have high value of activation energy and vice versa [33].The high value of activation energy depends upon the high absorption value of RE ions??. The conduction mechanism elaborates interference between metal and metallic ions??. It has been represented that the increase in ionic distance?? increases lattice constant. The increase in lattice constants increases activation energy consequently??? [34, 35].

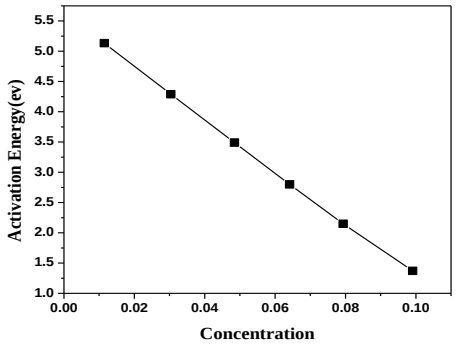

Fig. 5. Activation Energy for $Ca_{0.5-x}Ba_{0.5}In_xMn_yFe_{12-y}O_{19}$ (x=0.00 – 0.10 and y= 0.0 -1.0).

4.3. DC conductivity

Fig. 6 shows the DC conductivity. It is clear from the plot that conductivity increases with temperature. It indicates that ferrites have semiconductors like behavior [36, 37].The conductivity in ferrites at room temperature is because of the impurity. The conductivity at high temperature is due to polaron hopping. This physical phenomenon within ferrites could also be explained by Verwey's hopping mechanism [38]. According to the Verwey model, the electronic conduction in ferrites is majorly because of hopping of electrons between ions of the same elements with variable valancies distributed randomly over crystallographic lattice sites (octahedral sites). The hopping probability directly depends on the distance (separation) between ions involved in conduction and the potential barrier that must be overcome known as activation energy for hopping.

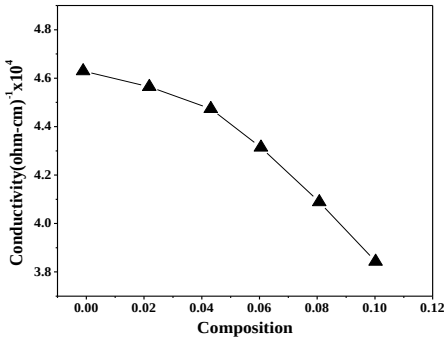

Fig. 6. DC Conductivity at room temperature for $Ca_{0.5-x}Ba_{0.5}In_xMn_yFe_{12-y}O_{19}$(x=0.00 – 0.10 and y= 0.0 -1.0).

Within the hexagonal arrangement there are two crystallographic sites A (tetrahedral) and B (octahedral). The distance between 2 metal particles at B-B sites is smaller than that of metals at B-A sites so the electron hopping between B-A sites has a very small probability than that for B-B sites. Hopping among A–A sites don't exist for the easy reason that there are unit exclusively Fe^{3+}

ions at A site and any Fe^{2+} ions fashioned throughout process preferentially occupy B sites. The hopping possibilities depend on the separation between ions concerned and the activation energy. So, at extreme temperature the hopping among $Fe^{2+} \leftrightarrow Fe^{3+}$ and $In^{2+} \leftrightarrow In^{3+}$ is increased which intern increases the DC conductivity [39].

4.4. Scanning Electron Microscopy (SEM)

Fig. 7 shows the SEM images that were observed for three selected samples at nominal composition $Ca_{0.5-x}Ba_{0.5}In_xMn_y\ Fe_{12-y}\ O_{19}$(x = 0.00 – 0.10 and y = 0.0 – 1.0). The SEM image indicates that the grains have well defined hexagonal shape and boundaries. The grain size calculated by SEM images was 10μm-1μm for $Ca_{0.5-x}\ Ba_{0.5}In_xMn_y\ Fe_{12-y}\ O_{19}$(x = 0.00 – 0.10 and y = 0.0 – 1.0) samples respectively. The grains are small enough and are suitable for better signal to noise ratio and memory devices. The grain size decreases with increasing In-Mn contents [40-45]. This decrease in grain size is obvious from the analysis that the stoichiometric amounts of Ca^2 and Fe^3 is decreased by increasing In^3, Mn^2 ions.

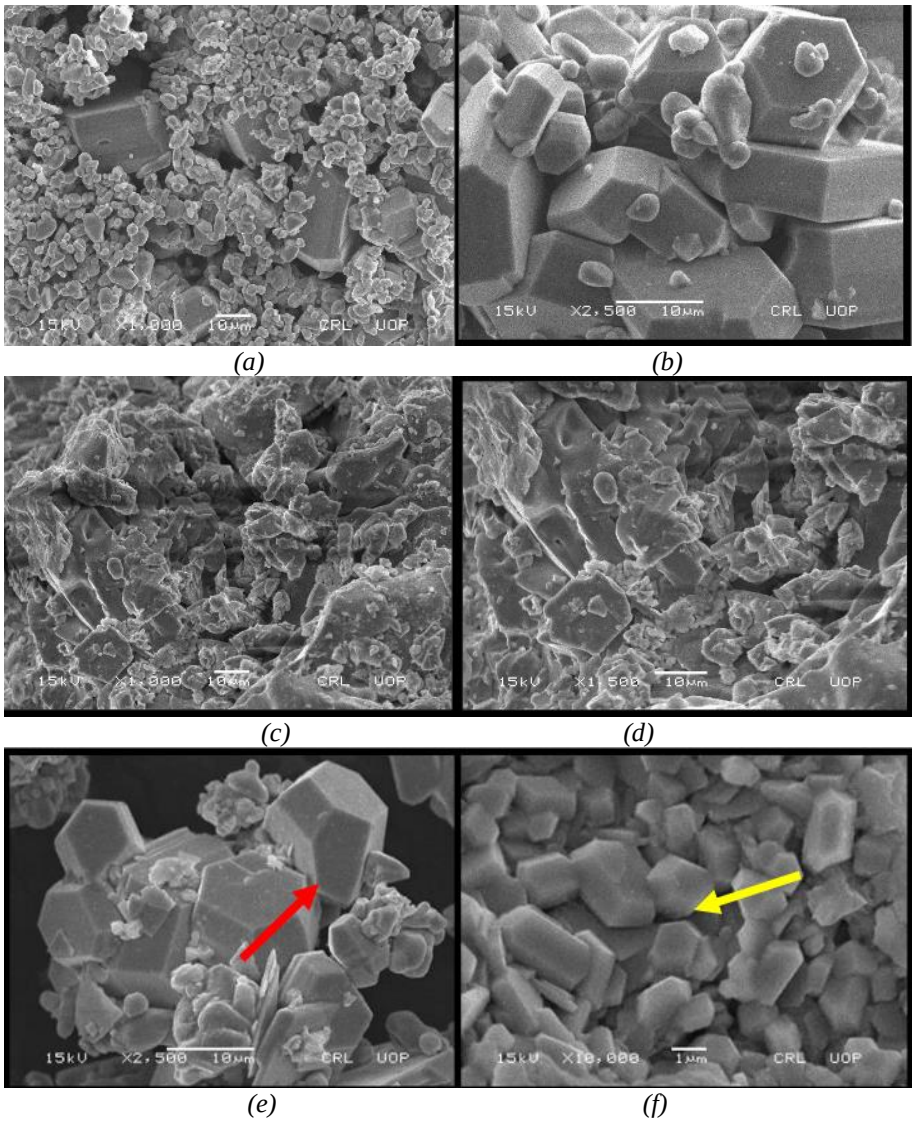

(a) *(b)* *(c)* *(d)* *(e)* *(f)*

Fig. 7. SEM (a -f) for $Ca_{0.5-x}Ba_{0.5}\ In_xMn_yFe_{12-y}O_{19}$(x=0.00 – 0.10 and y= 0.0 -1.0).

4.5. Dielectric Properties

4.5.1. Dielectric Constant

Fig. 8 shows the dielectric constant versus frequency for $Ca_{0.5-x}\,Ba_{0.5}\,In_x\,Mn_y\,Fe_{12-y}O_{19}$ (x = 0.00–0.10; y = 0.00–1.00) at room temperature. The dielectric constant decreases with increasing as shown in Fig. 8. At the high frequencies, the dielectric constant seems independent of frequency. This performance about the sample in according to Maxwell–Wagner model [46]. The Maxwell-Wagner model describes the dielectric constant of substance with non-homogenous composition can be composed of excellent conducting particle separated by extremely resistive thin particle boundaries [47]. During this case, the voltage applied on the sample drop mainly across the particle boundary and charge dispersion is established on the particle boundary. This space charge dispersion is ruled with the free offered charge at the small grain boundaries by physical phenomenon effective on sample. These actual effects on the ferrites, the charge dispersion directly depends on the Fe^{2+} particle during absorption and Mn^{2+}ions have to fill (In^{3+}) tetragonal A-sites. So concentrations of the Fe^{2+} ion on tetragonal site decreases. Hence, thanks to reduce in electrical dispersion, so the dielectric constant also decreases. This may add to the explanation that the In^{3+}ions failed to participate in the physical phenomenon method, however, impede the motion of charge carrier participate in the physical phenomenon method [48]. Koops explained the reduced frequencies are dominant at impact of small grain boundaries i.e. high dielectric constant for nearly small thin grain boundaries. Higher dielectric constants reduce the observation intensity of effective magnetic force then magnetic waves due to raising the electrical phenomenon. Then, abundant lower dielectric constants obtain for the ferrites deserve their application at high frequency [49].

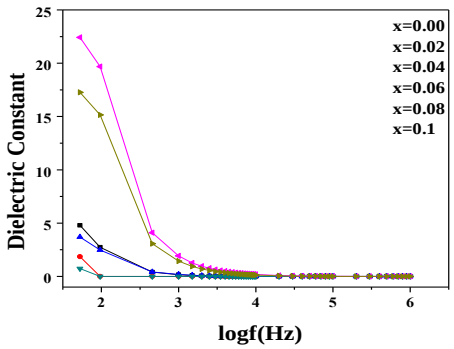

Fig. 8. Dielectric Constant versus frequency for $Ca_{0.5-x}Ba_{0.5}In_xMn_yFe_{12-y}O_{19}$ (x= 0.00-0.10; y = 0.00-1.00) Hexaferrites.

4.5.2. Dielectric loss

Fig. 9 shows dielectric loss versus frequency for $Ca_{0.5-x}Ba_{0.5}In_x\,Mn_yFe_{12-y}O_{19}$ (x = 0.00–0.10; y = 0.00–1.00) ferrites. The dielectric loss is main part of the entire core loss inside magnetic substance. Hence, low dielectric loss and unit area admirable. With increasing frequency the dielectric loss decreases and come to constant value [50].The dielectric losses represent the energy scattering within the dielectric system. It can be attributable to the decrease within Fe^{2+} particles absorption, due to dependable for conduction losses as a result of In^{3+} and Mn^{2+}contents as explain in the earlier paper [51]. Grain boundaries are developed in higher resistance due to low-frequency region, the external energy is required due to exchange of electrons between Fe^{3+} and Fe^{2+} ions, which result in higher dielectric loss. Smaller energy is required for conductions of electron transfer from ferric to ferrous atoms within the grain, so the energy losses are reduced.

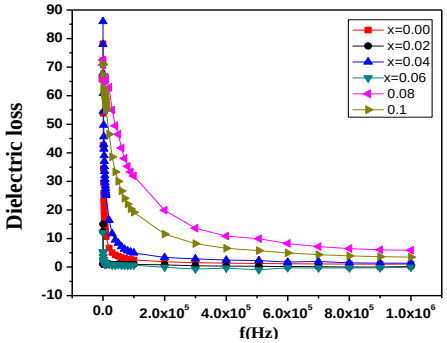

Fig. 9. Dielectric loss versus frequency for $Ca_{0.5-x}Ba_{0.5}In_xMn_yFe_{12-y}O_{19}$ (x= 0.00 - 0.10; y = 0.00-1.00) Hexaferrites.

5. Conclusions

The samples ($Ca_{0.5-x}Ba_{0.5}In_xMn_yFe_{12-y}O_{19}$ (x= 0.00-0.10; y = 0.00-1.00) prepared by sol – gel auto combustion method results in enhanced Structural, electrical and Dielectric Properties.

XRD patterns of samples ($Ca_{0.5-x}Ba_{0.5}In_xMn_yFe_{12-y}O_{19}$ (x= 0.00-0.10; y = 0.00-1.00) indicates that the peaks match well with the Standard Pattern of M – Type hexaferrites compared with (JCPDS card No.01-078-0132).Lattice parameter lies in the range a = 5.386Å – 5.892Å and c =23.201Å – 23.502Å. SEM indicates well defined and homogenized shapes of the hexaferrites. Resistivity ranges from $2.0x10^6$ Ω-cm to $5.2x10^6$Ω-cm. The hopping possibility at room temperature depends upon the separation between ions concentration and activation energy. According to the Maxwell–Wagner model, the dielectric material contains with heterogeneous arrangement throughout the substance can be composed of good conducting particles separated by highly resistant thin grains boundaries. Dielectric loss is the very important part of the small core loss in magnetic substance. It appears from the result that the binary mixture of (In-Mn) ions can be used to control the electric behavior of the Calcium -Barium (Ca-Ba) hexaferrite nanoparticles, while conduction for $Ca_{0.5-x}Ba_{0.5}\ In_x\ Mn_yFe_{12-y}O_{19}$(x= 0.00-0.10; y = 0.00-1.00) is explained by the hopping conduction mechanism of localized charge carrier.

References

[1] G. Albnese, A. Dariu, F. Licci, S. Rinaldi, IEEE Trans. Magn. **14**, 710 (1978).
[2] H. J. Kown, J. Y. Shin, J. H. Oh, J Appl Phys **75**, 6109 (1994).
[3] E. Naiden, V. Maltsen, G. Ryabtsen. Phys Stat Sol **120**, 209 (1990).
[4] K. Yoon, D. Lee, H. Jung, S. J. Yoon, Mater Sci **27**, 2941 (1992).
[5] J. Ding, D. Maurice, W. F. Miao, P. G. McCormick, R. Street, J. Magn Magn Mater **150**, 417 (1995).
[6] G. Mendoza Suarez, J. A. Matutes-Aquino, J. I. Escalante-Garcıa, H. Mancha-Molinar, D. Rios-Jara, K. K. Johal, J Magn Magn Mater **223**, 55 (2001).
[7] S. M. Abbas, A. K. Dixit, R. Chatterjee, T. C. Goel, J Magn Magn Mater **309**, 20 (2007).
[8] J. Kulikowski, J Magn Magn Mater **41**, 56 (1984).
[9] S. Ruan, B. Xu, H. Suo, F. Wu, S. Xiang, M. Zhao, J Magn Magn Mater **212**, 175 (2000).
[10] Hasan M. Khan, M. U. Islam, Yongbing Xu, M. Asif Iqbal, Irshad Ali, Journal of Alloys and Compounds **589**, 258 (2014).
[11] Ramasamy DSR In: International conference electromagnetic interference and compatibility (INCEMIC-97), NeJersey 7B-7,(1997) p 459.
[12] M. A. El Hiti, J Magn Magn Mater **192**, 305 (1996).
[13] Hasan M. Khan, M. U. Islam, Yongbing Xu, Irshad Ali, M. AsifIqbal, M. Ishaque, Muhammad Azhar Khan, Nazia Karamat, Imran Sadiq, Springer Science **0928**, 0707 (2015).
[14] R. Valanzuela, (2005) Magnetic ceramics. Cambridge University Press, Cambridge

[15] M. J. Iqbal, M. N. Ashiq, Chem Eng J **136**, 383 (2008).
[16] M. U. Islam, F. Aen, S. B. Niazi, M. Azhar Khan, M. Ishaque, T. Abbas, M. U. Rana, Mater Chem Phys **109**, 482 (2008).
[17] C. Kittel, Introduction to Solid State Physics, John Wiley & Sons (Asia), Singapore, (1996).
[18] H. M. Khan, M. U. Islam, Y. Xu, M. N. Ashiq, I. Ali, Asif Iqbal, M. Ishaque, Ceram Intl **40**, 6487 (2014).
[19] H. M. Khan, M. U. Islam, Y. Xu, M. A. Iqbal, I. Ali, J Alloys Compd **589**, 258 (2014).
[20] S. Sindhu, M. R. Anantharaman, B. P. Thampi, K. A. Malini, P. Kurian, Bull Mater Sci **25**, 599 (2002).
[21] B. D. Cullity, Element of X-ray Diffraction, 2nd ed., pp. 88, 284,(1978) 502.
[22] M. J. Iqbal, R. A. Khan, J. Alloys Compd. **374**, (2862009).
[23] T. W. Lambe, Soil Testing for Engineers, John Wiley and Sons, Inc., New York, (1951) p. 165.
[24] A. Pradeep, G. Chandrasekaran, Materials Letters **60**, 371 (2006).
[25] The absorption of some metal oxides with spinel structure, Zeitschrift Fur Crystallography **115**, 331 (1961).
[26] R. D. Waldron, Physical Review **99**, 1727 (1955).
[27] P. Xu, X. J. Han, M. J. Wang, J. Phys. Chem. C **111**, 5866 (2007).
[28] Joint Committee Powder Diffraction Fiels (JCPDF) Card No. 84- 0757.
[29] M. N. Ashiq, M. J. Iqbal, I. H. Gul, J. Alloys Comp. **487**, 341 (2009).
[30] N. Rezlescu, C. Doroftei, E. Rezlescu, P. D. Popa, Phys. Status Solidi **15**, 3844 (2006).
[31] T. R. Wagner, J. Solid State Chem. **136**, 120 (1998).
[32] S. Che, J. Wang, Q. Chen, J. Phys Condens Matter **15**, L335 (2003).
[33] B. Ramesh, D. Ravinder, Materials Letters **62**, 2043 (2008).
[34] E. Rezlescu,N. Rezlescu, P.D. Popa, L. Rezlescu, C. Pasnicu, Physica Status Solidi A, 672 (1997).
[35] A. A. Sattar, Egyptian Journal of Solids **26**(2), 113 (2003).
[36] T. Abbas, M. U. Islam, M. A. Chaudhry, Mod. Phys. Lett. B **9**(22), 1419 (1995).
[37] J. Smit, H. P. J. Wijn, Ferrites, Wiley, New York, (1959).
[38] E. J. W. Verwey, J. H. De Boer, Rec. Trans. Chem. Des. Pays. Bas. **55**, 531 (1936).
[39] A. Lakshman, P. S. V. SubhaRao, B. P. Rao, K. H. Rao, J. Phys. D. Appl. Phys. **38**, 673 (2005).
[40] Deschamps, F. Bertaut, Comp. Rend. Acad. Sci. **17**, 3069 (1957).
[41] S. W. Lee, S. Y. An, I. Shim, C. S. Kim, J. Magn. Magn. Mater. **231**, 290 (2005).
[42] M. M. Rashad, M. Radwan, M. M. Hessien, J. Alloy Comp. **453**, 304 (2008).
[43] C. Mu, N. Chen, X. Pan, X. Shen, X. Gu, Mater. Lett. **62**, 840 (2008).
[44] H. Khan, M. Islam, I. Ali, M. U. Rana, Mater. Sci. Appl. **2**(8), 1083 (2011).
[45] Muhammad Javed Iqbal, Muhammad Naeem Ashiq, Iftikhar Hussain Gul, J. Magn. Magn. Mater. **322**, 1720 (2010).
[46] M. J. Iqbal, S. Farooq, Mater Chem Phys **118**, 308 (2009).
[47] M. A. Ahmed, E. Ateia, S. I. El-Dek, Mater Lett **57**, 4256 (2003).
[48] N. Rezlescu, E. Rezlescu, C. Pasnicu, M. L. Craus, J Phys Codens Matter **6**, 5707 (1994).
[49] M. K. Shobana, S. Sankara, V. Rajendran, Mater Chem Phys **113**, 10 (2009).
[50] V. R. K. Murthy, J. Shobanadri, Phys Status Solid A **36**(2), 133 (1976).
[51] K. W.Wagner, Ann Phys **40**, 817 (1913).